Additive Manufacturing 24 (2018) 13–19

Contents lists available at ScienceDirect

Additive Manufacturing

journal homepage: www.elsevier.com/locate/addma

# Repercussions of powder contamination on the fatigue life of additive manufactured maraging steel

A. Gatto, E. Bassoli, L. Denti*

*Department of Engineering "Enzo Ferrari", University of Modena and Reggio Emilia, via Vivarelli 10, 41125 Modena, Italy*

ARTICLE INFO

*Keywords:*
Maraging
18Ni-300
Fatigue life
Powder bed fusion
Cross-contamination

ABSTRACT

A wide range of materials is suitable for processing by powder bed fusion (PBF) techniques. Among the latest formulations, maraging steel 18Ni-300, which is a martensite-hardenable alloy, is often used when both high fracture toughness and high strength are required, or if dimensional changes need to be minimised. In direct tooling, 18Ni-300 can be successfully employed in numerous applications, for example in the production of dies for injection moulding and for casting of aluminium alloys; moreover, it is particularly valuable for high-performance engineering parts.

Even though bibliographic data are available on the effects that parameters, employed in PBF processes, have on the obtained density, roughness, hardness and microstructure of 18Ni-300, there is still a lack of knowledge on the fatigue life of PBF manufactured parts. This paper describes the fatigue behaviour of 18Ni-300 steel manufactured by PBF, as compared by forging. Relevant negative effects of the cross-contamination of the raw material are originally identified in this paper, which emphasizes the inadequacy of current acceptability protocols for PBF powders. In the absence of contamination, endurance achieved by PBF is found equal to that by forging and consistent with tooling requirements as set out by industrial partners, based on injection moulding process modelling.

## 1. Introduction

Maraging steels are renowned for their ability to put together different important properties of the material: they show both high strength and toughness and, at the same time, they are easily weldable and dimensionally stable while ageing by heat treatment. As an example, 18Ni-350 has strength up to 2400 MPa, while 13Ni-400 up to 2800 MPa [1,2]. Maraging steels, containing 18% Ni, are grouped into two large sets, according to which chemical component represents the leading reinforcing agent. One group is cobalt strengthened (7–12% Co) and the corresponding steels are known as C-type steels. In the second group, in which cobalt is not present, steels are titanium strengthened and they are called T-type. In both sets, there is a further categorisation of steels as 200, 250, 300 and 350 grades, based on their level of tensile strength [2].

Ultra-high strength is a desired property of steel, possessed by maraging steels, which in fact show unique combinations of very high resistance, obtained through precipitation hardening. On the other hand, these alloys lack of fatigue strength: with respect to endurance, maraging steels show results that are much lower than those expected and predicted via empirical methods, by which fatigue limit is usually estimated around half of the ultimate tensile strength. Little residual stresses are commonly present in ultra-high strength and heat treated steels, as well as, even, the clustering of hydrogen atoms laid out near non-metallic inclusions [3]. The application of cyclic loads, superimposed with the mentioned residual stresses and hydrogen atoms presence, leads to hydrogen-assisted cracking, which is the formation and growth of cracks alongside inner non-metallic inclusions [3].

In order to become hardened, maraging steels undergo a metallurgic reaction, involving no carbon, which makes them different from conventional steels. The lattice is hardened as a result of inter-metallic compounds precipitating at a temperature value around 480 °C [4]. Since the austenite to martensite transformation takes place at a fairly low temperature (the martensite transformation of the 250 grade maraging steel starts at approximately 154 °C), which is an obstacle to diffusion controlled processes, the martensite forms via a diffusionless shear process. An important practical benefit is that martensite is formed at all cooling rates and therefore in all the sections of a specimen [5]. The hardness value increases according to the increase in the ageing temperature and time. However, a plateau appears in the "hardness versus ageing temperature and time" curve, and limit values are present. Mechanical performances decrease beyond these limits.

* Corresponding author.
*E-mail addresses:* andrea.gatto@unimore.it (A. Gatto), elena.bassoli@unimore.it (E. Bassoli), lucia.denti@unimore.it (L. Denti).

https://doi.org/10.1016/j.addma.2018.09.004
Received 13 May 2018; Received in revised form 4 September 2018; Accepted 4 September 2018
Available online 06 September 2018

Care should be taken in choosing ageing parameters: they should preclude over-ageing conditions, since a needlessly long ageing time yields formation of reverse transformed martensite, with a consequent decrease in strength and fatigue life [1].

Shot peening is the most common surface treatment of metal parts produced via PBF technique.

This treatment leads to residual stresses on the surface that have compressive nature and are quite strong (around 600 MPa), thus exerting a favourable effect towards the fatigue life of the fabricated items [6]. Literature data report values of surface roughness $R_a$ = 4–6.5 μm for 18Ni-300 PBF manufactured and shot-peened specimens [7].

As evidenced in [8], in the case of maraging steel, reducing the roughness below a 5 μm threshold, by surface polishing, does not increase the resistance to fatigue, due to the presence of small inclusions.

High cooling rates accompany selective laser melting of materials. As a consequence, non-equilibrium phases may form, including quasi-crystalline ones, or new crystal phases characterised by a wide composition gamma [9]. If the cooling velocity is large enough, structures may be noticed that are finer than in the case of conventional manufacturing techniques; furthermore, during the solidification process, gas bubbles may get entrapped in the material, as well as oxide inclusions. Therefore, the properties of parts built via additive manufacturing (AM) may differ from those fabricated by conventional techniques [9]. Several studies on the properties of PBF manufactured items are available; most of them focus on the characteristics (microstructure, porosity, roughness, hardness) resulting from manufacturing and post-process parameters. But only in very few works is attention given to phenomena and parameters that could affect the lifespan of the parts and might lead to an early breakdown of the used components [6].

Quality and endurance of additive manufactured (AM) components should be investigated carefully to offer more insights to those designers who employ this technology. The introduction of tool steel formulations among the range of materials for PBF systems opened the strategic application field of mould inserts with conformal cooling channels. When CAE modelling of the injection moulding process points out areas where the cooling is slow, the design of cooling channels that run just below the active surface may result in high competitiveness in moulds requiring extreme productivity, with reductions of the cooling time as impressive as 50%. In this field, traditional subtractive processes and additive laser-based ones are often combined for the production of each mould insert. This allows the minimization of costs, since every simple bulky part of the mould is machined, whereas small complex inserts with conformal channels are produced by PBF with little material usage and low cost. Packaging is the first end-market of such solutions, where a mould can produce up to 200 parts per minute, costs up to 500,000 € and requires two man-months for the development. The great added-value of the described approach is currently hampered by the quality variance and long-term unreliability of the mould-inserts, which are intolerable for such a demanding application. Based on CAE modelling of the injection moulding process, fatigue limit requirements can be at a maximum stress of 400 MPa.

Our research has thus focused on understanding the behaviour under cyclic load conditions of 18Ni-300 finished specimens fabricated via the PBF technique, as compared with forging that represents the traditional industrial solution for mould-makers.

Tests have been carried out to correlate the maximum stress to the number of cycles to failure.

An optical microscope, a scanning electron microscope and Energy Dispersive X-ray (EDX) analysis have been utilised to analyse initiation and propagation of cracks. Results show that the powder characteristics may determine the performance of the additive manufactured parts and that powder cross-contamination may have dramatic effects on the final output. Effects of the raw powder characteristics on the fatigue properties are discussed in Section 3. Controlling the properties of the powder, employed in metal-based AM, represents an industrial task, fundamental towards making a safe powder choice and building components that are consistent and possess known and predictable features [10].

**Table 1**
Specimens considered in the experimental plan.

| Designation | No. of specimens | Material | Technology | Standard | Age hardening |
|---|---|---|---|---|---|
| $T_{Additive1}$ | 4 | 18Ni-300 | PBF | ASTM E466 | 6 h at 490 °C |
| $T_{Additive2}$ | 2 | | | | |
| $T_{Forged}$ | 5 | | FORGING | | |

Additive1 = powder from lot 1.
Additive2 = powder from lot 2.

## 2. Materials and methods

Maraging steel powder was used to produce samples by PBF, and equivalents for comparison have been manufactured by forging using the same alloy (Table 1).

Tensile static and fatigue specimens were manufactured, machined and finished by grinding to the geometry shown in Fig. 1 (ASTM E466 standard). Fatigue specimens were made by PBF using powder taken from two separate, nominally equivalent lots. All specimens were heated to 490 °C for 6 h, following data reported in the literature.

A crosshead speed of 2 mm/min was employed in the static tensile tests developed to assay ultimate tensile strength (UTS) and select the stress values to be used in the fatigue tests.

Axial fatigue tests were performed using the following parameters:

- constant amplitude of load and unidirectional stress (R = 0);
- maximum stress values set to 250, 350 and 500 MPa;
- limit value of infinite life, set to $5 \times 10^6$ cycles;
- frequency of 6 Hz and sinusoidal load.

The choice of frequency was a compromise between the need for a low time-consuming test and a low frequency, to avoid an apparent increase in the lifespan. Results depend on the frequency when a strain rate dependency exists in the behaviour of the material, as in the case of precipitation hardening: the fatigue life tends to increase as the frequency increases [11,12].

Given the relevance of surface finish to fatigue life [13,14], roughness was measured using a Diavite DH5, with a measurement length $l_m$ and a cut-off length $l_c$ respectively of 4.8 and 0.8 mm. Five measurements were performed in parallel direction with the specimen axis, and five were conducted perpendicular to the specimen axis. To evaluate if the finishing steps had any effect of surface heating and change of the microstructure, a cross-section of a specimen was metallographically prepared, and the micro-hardness was mapped through the thickness. Nominal powder and forged specimen compositions were provided by the manufacturer (R.B. S.r.l, Modena, Italy), confirmed through EDX analysis and reported in Table 2. Specimens produced using PBF were built with EOSINT 270 (EOS GmbH Electro-Optical System) using standard process parameters, as shown in Table 3. Expected mechanical performances are listed in Table 4. Optical and scanning electron micrographs and EDX analysis were utilised to compare and analyse crack initiation and propagation characteristics. Influence of defects on fatigue properties is discussed, based on results.

## 3. Results and discussion

Roughness values (mean and standard deviation) of the specimens are shown in Table 5 for both directions, parallel (longitudinal) and perpendicular (transversal) to the specimen axis. Roughness achieved for the specimens produced by PBF and by forging is equivalent.

Hardness maps measured on cross-sections of a forged and of a PBF manufactured sample are shown in Fig. 2. A supplementary box plot

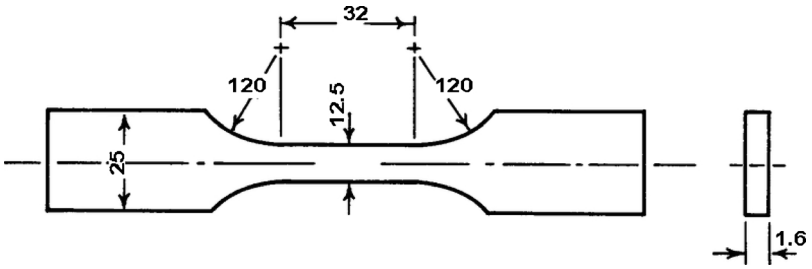


**Fig. 1.** Geometry of the tensile static and fatigue specimens (ASTM E466).

comparison of ranges measured for the two types of specimens is given in Fig. 1 in [15]. Hardness of the additive specimen is almost constant throughout the thickness, in the range 510–550 HV. It decreases for the forged specimen, as we go from the machined surface towards the specimen core, likely due to different strain-hardening conditions. No relevant effect of the grinding process is observed.

Results of the static tensile tests are listed in Table 6, where the average and standard deviation of 5 test repetitions are reported. Example stress-strain curves are shown In Fig. 2 in [15]. PBF manufactured specimens and forged ones show almost the same UTS. Tensile strength is also very similar to the expected value in the technical datasheet.

Results of fatigue tests are listed in Table 7 and depicted in Fig. 3. Rupture sporadically occurred in an irregular way, as detailed in [1], and the associated tests were excluded from the results. Stress-life plot shows that, under the same load condition, the lifespan of forged specimens is in many cases longer than that of additive manufactured specimens. However, at a deeper look, it can be remarked that performance related to PBF produced samples is conflicting. With the first powder batch, even a stress level as low as 250 MPa (13% of UTS) causes an extremely early failure at $2 \times 10^5$ cycles; whereas infinite life is shown at $\sigma_{max} = 400$ MPa by two specimens produced with the second powder batch. The latter results are actually even superior to the endurance of forged specimens. These contradictory data suggested that a careful analysis of the rupture surfaces was necessary.

SEM observations of $T_{Additive1}$ specimens point out the frequent presence, at failure initiation sites, of inclusions (Fig. 4) that are distinct from the phase in which they are embedded. EDX analysis of the inclusions has revealed the presence of Ti and Al oxides, while the matrix shows the presence of Fe, Ni, Co and Mo. Fig. 4 clearly shows that the pollutant generates a defect that initiates part failure. Numerous cracks, propagating along radial directions, start from the spherical inclusion. In this case, yield and tensile strength are equal to the nominal value, but fatigue life for a maximum stress of 26% of UTS is as short as $10^4$ cycles. Some other authors have also observed numerous $Al_2O_3$ and $TiO_2$ inclusions in 18Ni-300 produced by PBF technique [4]. Microporosities are sometimes visible around the inclusions, as in Fig. 5. Compared with the steel matrix, these ceramic phases have a smaller thermal expansion coefficient (see Table 8), and there exists the hypothesis of a tensile residual stress at equator lines of ceramic inclusions [3,16,17]. Some works have verified [3] that inclusion interfaces could trap hydrogen atoms. In these works, the authors' assumption was that cracks initiated and grew from inner non-metallic inclusions, as a consequence of superposition of the applied cyclic load with residual stress and at the presence of hydrogen. In the case of maraging steel, the hypothesis can thus be made on fatigue cracking to be caused by inner inclusions even under low stress values [3]. This paper confirms such a conclusion for AM parts and points out that the fatigue rupture mechanisms are similar to those of a bulk material, but phenomena get emphasised by external factors, that increase the presence of inclusions (for example, the powder supply chain).

No inclusions or local variations of chemical composition were detected on the rupture surfaces of the two $T_{Additive2}$ specimens that reached infinite life for the maximum stress of 400 MPa.

Some authors have reported that the entire fatigue fracture surface of 2.8 GPa grade maraging steel can be separated into three distinct areas: a flat zone, bordered by a most internal semielliptic profile; a sandwich region, enclosed within paired semielliptic lines and characterised by a definite coarse morphology; a large fracture surface, crossed by several radial ridges along the crack direction of propagation [3]. Fig. 6 shows the rupture surface of a forged specimen: the crack surface may be subdivided into three regions, according to observations by Wei Wang et al. [3], but the morphology of the crack surface differs

**Table 3**
Parameters related to PBF manufacturing.

| | | |
|---|---|---|
| Laser power | [W] | 200 |
| Laser spot diameter | [mm] | 0.2 |
| Scan speed | [m/s] | ≤7.0 |
| Building speed | [$mm^3$/s] | 2–20 |
| Layer thickness | [mm] | 0.02 |
| Protective atmosphere | [% oxygen] | ≤1.5 |
| Scan strategy | Island hatching, 25° rotation at each next layer | |

**Table 4**
Material datasheet for physical and mechanical properties [7].

| | | |
|---|---|---|
| Density | [$kg/dm^3$] | 8.0–8.1 |
| UTS | [MPa] | 1930 |
| Rp0.2 | [MPa] | 1862 |
| Elongation at break | | 2% |
| Young's Modulus | [GPa] | 180 |
| HV* | | 513–613 |

* Converted from HRC values.

**Table 5**
Roughness measured for AM and forged specimens used in the axial fatigue test.

| | | $T_{Additive1}$ | | $T_{Forged}$ | |
|---|---|---|---|---|---|
| | | MEAN | SD | MEAN | SD |
| $R_{a,\ longitudinal}$ | [μm] | **1.14** | 0.06 | **0.86** | 0.14 |
| $R_{a,\ transversal}$ | [μm] | **0.51** | 0.04 | **0.482** | 0.02 |
| $R_{max,\ longitudinal}$ | [μm] | **7.96** | 1.25 | **7.16** | 0.87 |
| $R_{max,\ transversal}$ | [μm] | **4.36** | 0.49 | **4.2** | 0.56 |

**Table 2**
Nominal composition of the studied alloy (wt.%) determined by EDX analysis.

| Fe | Ni | Co | Mo | Ti | Al | Cr, Cu | C | Mn, Si | P, S |
|---|---|---|---|---|---|---|---|---|---|
| bal | 17–19 | 8.5–9.5 | 4.5–5.2 | 0.6–0.8 | 0.05–0.15 | ≤0.5 | ≤0.03 | ≤0.1 | ≤0.01 |

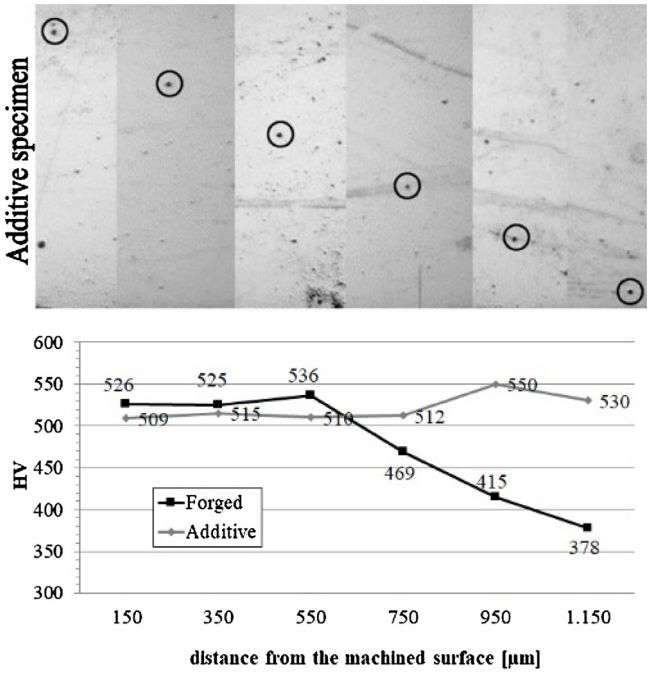


**Fig. 2.** Hardness maps of cross-sections of an additive manufactured and of a forged specimen. Hardness imprints are rounded by black circles in the micrographs.

**Table 6**
Static tensile test results: average and standard deviation (between brackets).

| | UTS [MPa] |
|---|---|
| $T_{Additive}$ | 1910 (26) |
| $T_{Forged}$ | 1940 (15) |

**Table 7**
Results of axial fatigue tests.

| Maximum stress [MPa] | Cycles to failure | | |
|---|---|---|---|
| | $T_{Additive1}$ | $T_{Additive2}$ | $T_{Forged}$ |
| 500 | $6.4{\cdot}10^4$ $5.9{\cdot}10^4$ | $4.6{\cdot}10^4$ | $9.4{\cdot}10^4$ $8.8{\cdot}10^4$ |
| 400 | | infinite life infinite life | |
| 350 | $1.7{\cdot}10^5$ | | $5.1{\cdot}10^5$ infinite life |
| 250 | $2.3{\cdot}10^5$ | | |

from that described by these authors. The first area, close to the initiating point of the crack, is shown in Fig. 6a. Fatigue marks and numerous secondary cracks are visible. The second area displays a transgranular failure, with a few secondary cracks and marks that are probably rubbing traces, but no fatigue striation is visible (Fig. 6b). The third area is characterised by microvoid coalescence (Fig. 6c).

The rupture surface morphology of the specimen produced by the AM technique (Fig. 7) is different from that obtained by forging. Fig. 7a shows the starting point of the crack, on which an inclusion rich in Ti and Al is detected. Tear ridges radiate from the inclusion; a few secondary cracks, close to the initiating spot, are visible in Fig. 7b, as well as fan-shaped radial marks and texture changes associated with the origin. The crack morphology changes, moving away from the starting point. A transgranular rupture mode is visible in Fig. 7c.

After the identification of inclusions as the cause for cracks, it was necessary to detect the origin of these foreign phases. The hypothesis was thus investigated of contamination from the so called “black powder”, which is the partially melted oxidized powder, aspirated in the workroom and collected by filtering. Black powder, however, collected and analysed by EDX, revealed a coherent composition to that of the virgin material without any traces of contaminant particles and, consequently, it was not possible to consider it as causing Ti and Al oxides. Raw powder was subjected to careful control via optical microscope observation: isolated particles of different colour were seldom noted. These particles were separated from the rest of the powder using a magnetised tip and were mounted onto a stub using a conductive glue. The amount of such particles was so small that recursive separation steps were needed, taking significant time and expert skill to develop. In both powder lots it was possible to detect and separate the described particles, which EDX analysis indicates contain Ti and Al, but no Fe, Co, Mo or Ni (Fig. 8). Additional examples are reported in [15]. Absence of Fe, Co, Mo and Ni is important, as it shows that these contaminants have a different origin from the steel powder. If the dark particle in Fig. 8 had originated from the fused material, which had undergone an inefficient mixing in the furnace before being atomised, some traces of Fe, Co and Ni would in fact have been expected. Therefore, it is possible to state that such particles were due to a cross-contamination.

Fatigue performances may be explained considering the following model: during laser exposure, titanium and aluminium react with the oxygen in the build chamber and form oxides. In fact, the gas atmosphere adopted in PBF machines for the production of steel is much less protective than required for building Ti and Al alloys. Oxides are solid in a metal melt pool; the matrix does not wet the oxides, leading to crack initiation. Oxide presence has little effect on the static tensile properties, but it has a relevant influence on the fatigue life. When PBF parts fatigue life is lower than that of forged ones, this is due to pollution of the powder prior building process. However, it is difficult to identify powder contamination through traditional methods of analysis, as for example inductively coupled plasma (ICP) mass spectrometry. In

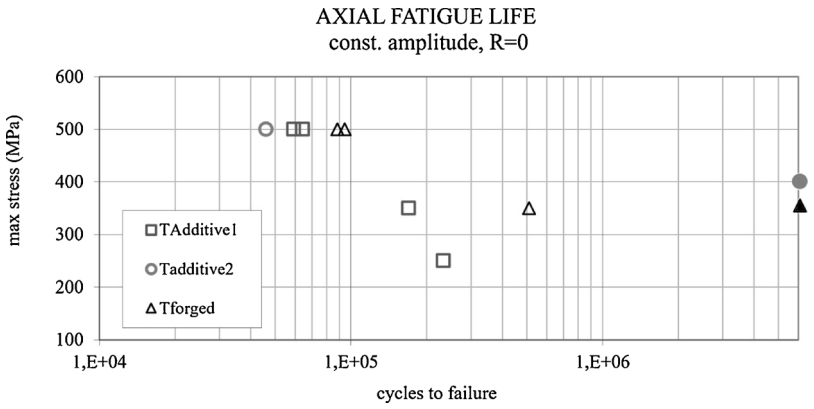


**Fig. 3.** Axial fatigue life. Run-outs are shown with filled markers.

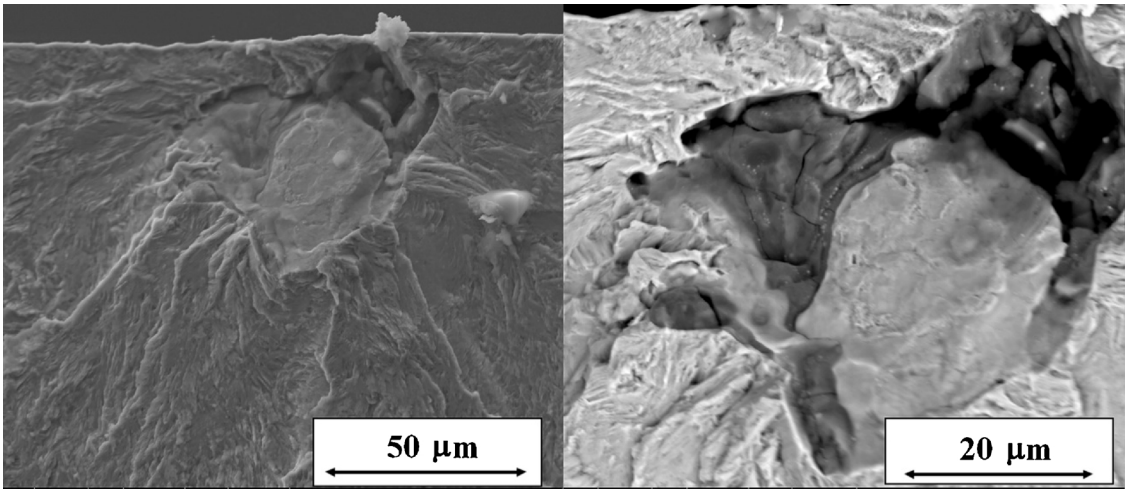


**Fig. 4.** Specimen $T_{Additive1A}$, $\sigma_{max}$ = 500 MPa, life = $5.9 \times 10^4$ cycles. EDX analysis of the inclusion reveals presence of O, Ti and Al. Tear ridges proceed radially from the inclusion. The image on the right shows an enlargement obtained using back-scattered electrons.

fact, a chemical analysis without previous separation procedures will average the composition over hundreds of microspheres. A single extraneous particle, thus, would leave the average composition unchanged, and consistent with the datasheet, especially if the contaminant is meant to be present as an alloying element. Yet, even a single contaminant particle may cause part failure. Chemical analysis does not allow the understanding of whether the weight percentage of Ti (for example), within the nominal range, is uniformly distributed as an alloying element or concentrated in a Titanium rich particle that will act as crack initiator. Neither flow tests or granulometric distribution, nor tensile tests, are helpful in spotting the presence of contaminants. As for tensile tests, this is due to the fact that the spheroidal inclusion cross-section was negligible with respect to the specimen section.

In the absence of contaminants, lifespan of parts produced by PBF can instead be equal to or even longer than for forged components. Parts produced by PBF technique show low repeatability for some physical properties: Sanz et al. [6] have affirmed that differences among samples should be attributed to the manufacturing process itself. This paper has shown that the differences may also be attributed to the condition of the initial powder.

## 4. Conclusion

Fatigue experiments have been carried out to evaluate the fatigue features of 18Ni-300 maraging steel specimens, produced using PBF technique. Results have been compared with those obtained from forged specimens. Rupture surfaces and virgin powder observations have revealed that contamination in steel powders, even by unalloyed constituents of the alloy, causes serious detriment to long-term behaviour. Early failures of mould-inserts produced in maraging steel by PBF may be ascribed to the presence of Ti alloy or Ti oxide particles in the raw material, probably due to supply chain glitches. On the contrary, fatigue endurance of PBF specimens that did not reveal the presence of contaminants was at least as high as of forged specimens. A few conclusions may be asserted, based on these observations, as follows.

**Table 8**
Thermal expansion coefficient of inclusions and matrix ($\times 10^{-6}$m/m K) [18–21].

| | 293 K | 500 K | 800 K |
|---|---|---|---|
| $Al_2O_3$ | 5.5 | 7.8 | 8.5 |
| $TiO_2$ | 7.5 | 8.4 | 9.3 |
| maraging steel | 9.7 | 10.08 | 10.08 |

- Contamination has a significant adverse influence on the fatigue life of 18Ni-300 specimens. Worrisome enough, the problem occurs even for percentages as small that the average chemical composition of the powder fits the nominal ranges. In these cases, the compositional anomaly is extremely localized, but sufficient to be detrimental.
- Standard quality control methods used for PBF powders, as for example the common ICP mass spectrometry, are inadequate for the detection of this type of raw material contamination. A prospective development of this study could be the investigation of microscopic computed tomography for the detection of contaminants.

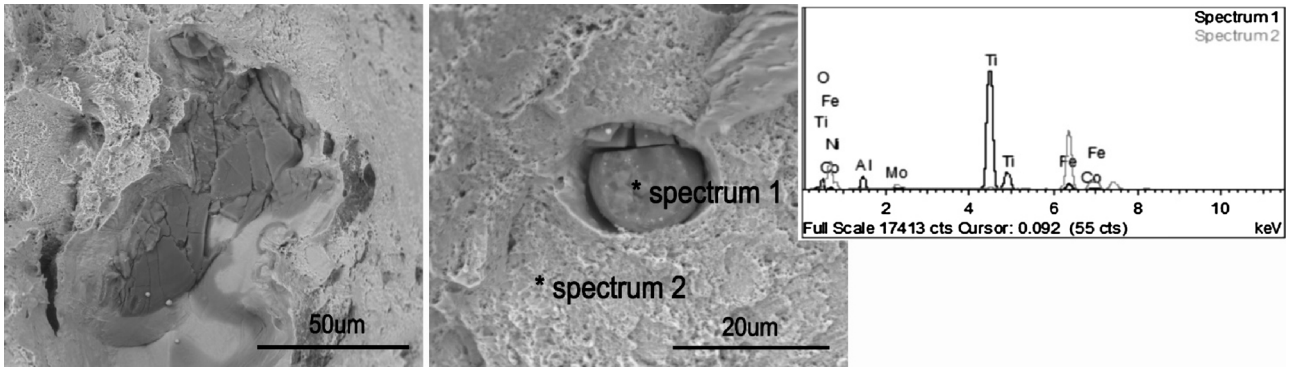


**Fig. 5.** Porosity around the inclusions on the rupture surfaces of static tensile tested additive specimens.

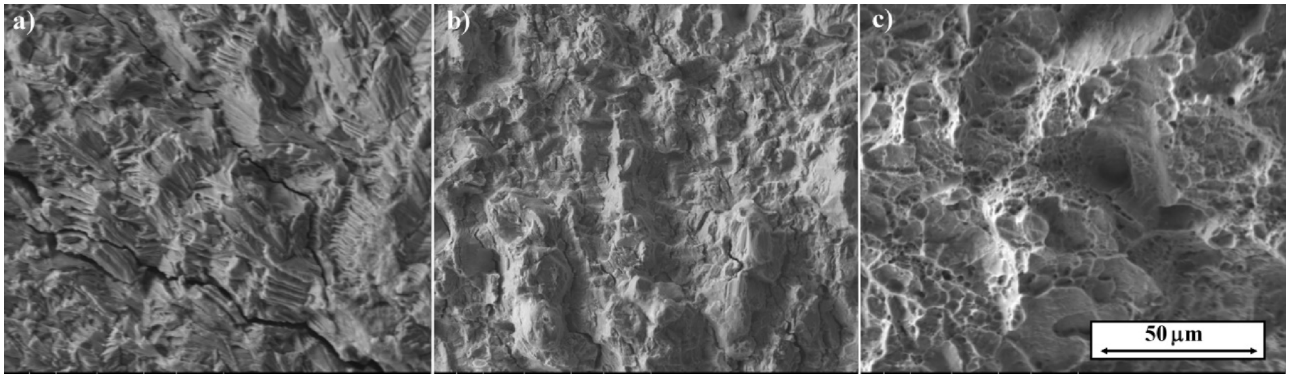


**Fig. 6.** $T_{Forged}$ specimen, $\sigma_{max}$ = 500 MPa, life = $9.4 \times 10^4$ cycles.

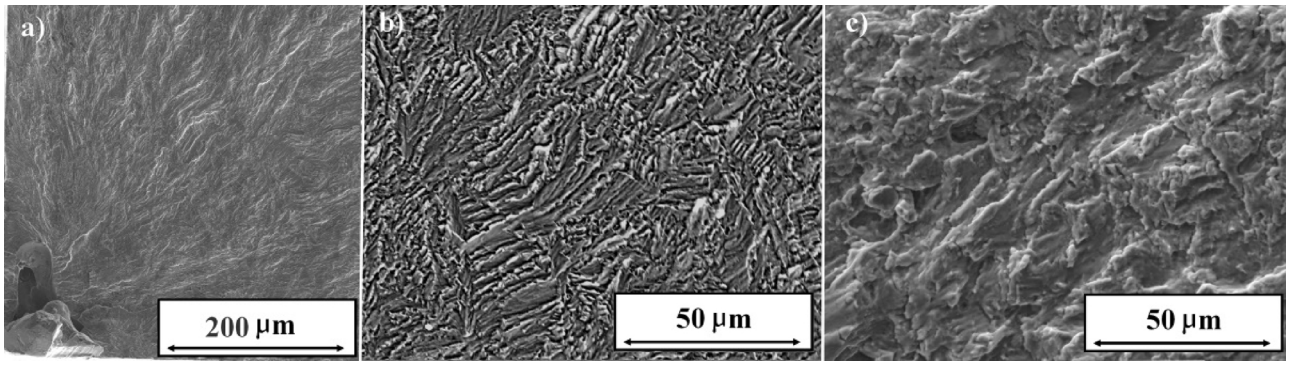


**Fig. 7.** $T_{Additive1B}$ specimen, $\sigma_{max}$ = 500 MPa, life = $6.4 \times 10^4$ cycles. a) An inclusion associated with porosity is detected at failure initiation point, in the left corner. EDX analysis of the inclusion confirms the presence of O, Ti and Al. Tear ridges radiate from the inclusion. b) A few secondary cracks, near the initiating spot, are visible, as well as fan-shaped radial marks. c) Transgranular rupture mode.

- Static tensile properties are unaffected by the presence of contaminants. The common validation procedure of jobs produced via PBF includes only static (and very rarely fatigue) tests, and it does not allow identification of whether a certain production batch is affected by problems as the ones studied in this paper. At least for steels, and as a safety check for other alloys, it is imperative to provide against these risks, especially for automotive, aircraft or prosthetic applications, where the consequences of part unreliability are not merely commercial.
- PBF specimens, produced using uncontaminated powder, can have the same (or even longer) fatigue life as the forged material.
- Low repeatability is shown for the fatigue behaviour of parts produced by PBF technique; according to some authors, the manufacturing process itself can be accounted for differences among samples; our work has pointed out that the differences may also be ascribed to the condition of the initial powder.
- The procedure employed in this study allows contamination occurrence to be identified, but it does not allow the percentage amount to be quantified.

## Declarations of interest

None.

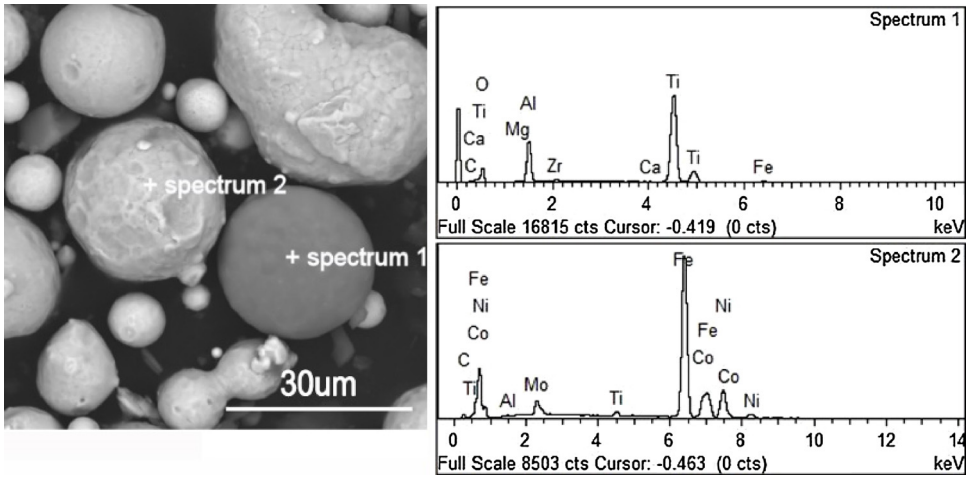


**Fig. 8.** Detection of contaminant particles in the raw powder used to produce $T_{Additive1}$ specimens.

## References


[1] D.G. Lee, K.C. Jang, J.M. Kuk, I.S. Kim, The influence of niobium and ageing treatment in the 18% Ni maraging steel, J. Mater. Process. Technol. 162–163 (2005) 342–349.
[2] Yi He, Ke Yang, Wenshen Qu, Fanya Kong, Su Guoyue, Strengthening and toughening of a 2800-MPa grade maraging steel, Mater. Lett. 56 (2002) 763–769.
[3] Wei Wang, Wei Yan, Qiqiang Duan, Yiyin Shan, Zhefeng Zhang, Yang Ke, Study on fatigue property of a new 2.8 GPa grade maraging steel, Mater. Sci. Eng. A 527 (2010) 3057–3063.
[4] E. Yasa, K. Kempen, J.-P. Kruth, L. Thijs, J. Van Humbeeck, Microstructure and mechanical properties of maraging steel 300 after selective laser melting, Solid Freeform Fabrication Symposium Proceedings (2010) 383–396.
[5] F.H. Lang, N. Kenyon: welding of Maraging steels, WRC Bulletin 159 (1971).
[6] C. Sanz, V. García Navas, Structural integrity of direct metal laser sintered parts subjected to thermal and finishing treatments, J. Mater. Process. Technol. 213 (2013) 2126–2136.
[7] EOS material data sheet, EOS Maraging Steel MS1.
[8] S. Usami, S. Shida, Elastic-plastic analysis of the fatigue limit for a material with small flaws, Fatigue Fract. Eng. Mater. Struct. 1 (1979) 471–481.
[9] K. Kempen, E. Yasa, L. Thijs, J.-P. Kruth, J. Van Humbeeck, Microstructure and mechanical properties of Selective Laser Melted 18Ni-300 steel, Phys. Procedia 12 (2011) 255–263.
[10] M. Seifi, A. Salem, J. Beuth, O. Harrysson, J.J. Lewandowski, Overview of materials qualification needs for metal additive manufacturing, JOM 68 (3) (2016) 747–764.
[11] B. Pyttel, D. Schwerdt, C. Berger, Very high cycle fatigue – is there a fatigue limit? Int. J. Fatigue 33 (2011) 49–58.
[12] T. Sakai, Review and prospects for current studies on very high cycle fatigue of metallic materials for machine structural us, J. Solid Mech. Mater. Eng. 3 (2009) 425–439 3.
[13] E. Brinksmeier, G. Levy, D. Meyer, A.B. Spierings, Surface integrity of selective-laser-melted components, Proc. CIRP (2010) 601–606.
[14] K.S. Chan, Characterization and analysis of surface notches on Ti-alloy plates fabricated by additive manufacturing techniques, Surf. Topogr.: Metrol. Prop. 3 (2015) 4.
[15] A. Gatto, E. Bassoli, L. Denti, Dataset on the observation of contaminants on the rupture surfaces of additively manufactured 18Ni-300 broken under fatigue stresses, Data Brief (2018) submitted.
[16] Y. Murakami, T. Nomoto, T. Ueda, Y. Murakami, On the mechanism of fatigue failure in the superlong life regime(N&107 cycles). Part I: influence of hydrogen trapped by inclusions, Fatigue Fract. Eng. Mater. Struct. 23 (2000) 893–902.
[17] Y. Murakami, T. Nomoto, T. Ueda, Factors influencing the mechanism of superlong fatigue failure in steels, Fatigue Fract, Nucl. Eng. 22 (7) (1999) 581–590.
[18] Dynamic Metals International, Maraging 300 datasheet.
[19] Maraging data sheet service steeel aerospace corp.
[20] Product Handbook of High Performances Alloys, Special Metals Corporation, 2008.
[21] ATI (Allegheny Technologies Incorporated) data sheet.